Mutation of Interfacial Residues Disrupts Subunit Folding and Particle Assembly of *Physalis mottle tymovirus**

Mahadevaiah Umashankar‡, Mathur R. N. Murthy§, and Handanahal S. Savithri‡¶

From the ‡Department of Biochemistry and the §Molecular Biophysics Unit, Indian Institute of Science, Bangalore 560 012, India

Virus-like particles (VLPs) serve as excellent model systems to identify the pathways of virus assembly. To gain insights into the assembly mechanisms of the *Physalis mottle tymovirus* (PhMV), six interfacial residues, identified based on the crystal structure of the native and recombinant capsids, were targeted for mutagenesis. The Q37E, Y67A, R68Q, D83A, I123A, and S145A mutants of the PhMV recombinant coat protein (rCP) expressed in *Escherichia coli* were soluble. However, except for the S145A mutant, which assembled into VLPs similar to that of wild type rCP capsids, all the other mutants failed to assemble into VLPs. Furthermore, the purified Q37E, Y67A, R68Q, D83A, and I123A rCP mutants existed essentially as partially folded monomers as revealed by sucrose density gradient analysis, circular dichroism, fluorescence, thermal, and urea denaturation studies. The rCP mutants locked into such conformations probably lack the structural signals/features that would allow them to assemble into capsids. Thus, the mutation of residues involved in inter-subunit interactions in PhMV disrupts both subunit folding and particle assembly.

Physalis mottle tymovirus (PhMV)[1] is a small spherical plant virus consisting of a single-stranded, plus-sense RNA genome with a size of 6.67 kb (1). The RNA genome is encapsidated in a protein shell comprising 180 chemically identical coat protein (CP) subunits (20,000 Da) arranged in icosahedral symmetry. Depending on the bonding interactions, the subunits are designated as A, B, and C (2). The A-type subunits form pentamers at the 5-fold, and the B and C subunits form hexamers at the 3-fold icosahedral axes. The protein subunits are held by strong protein-protein interactions.

Purified preparations of tymoviruses, including PhMV, consist of empty capsids (top component) in addition to the full capsids (bottom component) containing complete genomic RNA. An interesting feature of tymoviruses is that empty capsids are also formed *in vitro* when the intact virus is subjected to a freeze-thaw cycle or when exposed to high temperatures, alkaline pH, or denaturants (3–6). The presence of empty shells *in vivo* and *in vitro* suggests that the information required for error-free assembly is contained within the primary structure of protein subunits in these viruses. It is difficult to isolate an assembly-competent PhMV CP subunit under non-denaturing conditions from isolated viral capsids that can be used for deciphering the assembly pathway. Hence, the CP gene of PhMV and a number of its deletion mutants were cloned and expressed in *Escherichia coli.* Interestingly, the bacterially expressed rCP could self-assemble into stable virus-like particles (VLPs) (7). Furthermore, the deletion of 30 amino acid residues or the addition of 41 amino acid residues at the N terminus of rCP did not affect the assembly into T = 3 capsids. Several site-specific mutants were also studied. One of the mutations, His-69 to Ala, led to the formation of a 19.4 S subassembly intermediate (8). Recently, the crystal structures of native and recombinant capsids of PhMV have been elucidated (9, 10). To gain further insights into the assembly mechanism of this virus, a careful analysis of these crystal structures was made in the present study to identify residues involved only in inter-subunit interactions, and these residues were targeted for mutagenesis. Gln-37, Tyr-67, Arg-68, Asp-83, Ile-123 and Ser-145 were mutated to Glu, Ala, Gln, Ala, Ala, and Ala respectively, with a view to examine whether such mutations could lead to the formation of assembly intermediates or monomers. The mutant rCPs were expressed in *E. coli* and purified. The mutants were characterized by sucrose density gradient analysis, electron microscopy, high pressure liquid chromatography, circular dichroism (CD), and fluorescence spectroscopy. Our results imply that Gln-37, Tyr-67, Arg-68, Asp-83, and Ile-123 are not only important for assembly but also crucial for the proper folding of the subunits, whereas the interactions with Ser-145 are not important either for folding or assembly.

EXPERIMENTAL PROCEDURES

Materials—[α-^{32}P]dATP was obtained from PerkinElmer Life Sciences. Restriction endonucleases and the Sequenase™ Version 2 DNA sequencing kit were obtained from Amersham Biosciences. Deep Vent DNA polymerase, *Dpn*I, and Ni-NTA agarose were obtained from New England Biolabs and Qiagen, respectively. Ampicillin, isopropyl-1-thio-β-D-galactopyranoside, Coomassie Brilliant Blue R-250, and ultra-pure urea were obtained from USB. Diaminobenzidine, bromphenol blue, and EDTA were obtained from Sigma. The oligonucleotide primers and conjugated double antibodies were purchased from Bangalore Genei Pvt. Ltd., Bangalore, India. All other chemicals were of analytical grade.

Primers—The following primers were used to obtain rCP mutants by the PCR-based approach (-S, sense; -AS, antisense): Q37E-S, 5′-TCCC-TTTTGAGTTTGAAG-3′; Q37E-AS, 5′-CTTCAAACTCAAAAGGGA-3′; Y67A-S, 5′-CGCCCCCGCCCGACATGC-3′; Y67A-AS, 5′-GCATGTCG-GGCGGGGGCG-3′; R68Q-S, 5′-CCCCTACCAACATGCTCAG-3′; R68Q-AS, 5′-CTGAGCATGTTGGTAGGGG-3′; D83A-S, 5′-TCCAACT-GCTCTTGCTGTC-3′; D83A-AS, 5′-GACAGCAAGAGCAGTTGGA-3′; I123A-S, 5′-CGGCGCCGCCTCAGCCGCC-3′; I123A-AS, 5′-GGCGGC-TGAGGCGGCGCCG-3′; S145A-S, 5′-TTGAAAGACGCCGTGACCTAC-3′; and S145A-AS, 5′-GTAGGTCACGGCGTCTTTCAA-3′.

[1] The abbreviations used are: PhMV, *Physalis mottle tymovirus*; CP, coat protein; rCP, recombinant coat protein; CD, circular dichroism; Ni-NTA, nickel-nitrilotriacetic acid; ANS, 8-anilino-1-naphthalenesulfonate; T_m, melting temperature.

Effects of Interfacial Residue Mutations on PhMV

Site-directed Mutagenesis—The rCP mutants were constructed by the PCR-based method using corresponding sets of mutant primers (11). The wild type pRBCP (*i.e.* CP gene in pRSET-B vector) was used as the template for PCR amplification with the sense and antisense primers with 2.5 units of Deep Vent DNA polymerase under optimal conditions. The PCR-amplified mixtures were treated with *Dpn*I (10 units) at 37 °C for 1 h to digest the methylated template DNA and then transformed into *E. coli* DH5α-competent cells. The plasmid DNA isolated from the colonies was sequenced by Sanger's dideoxy chain termination method with a Sequenase™ Version 2.0 DNA sequencing kit to confirm the presence of the mutations.

Overexpression and Purification of Wild Type and Mutant rCPs—The wild type and mutant constructs were transformed into the BL21 (DE3) pLys S strain. 500 ml of Terrific broth containing 50 μg/ml ampicillin was inoculated with 1% of the preculture. After 4 h of growth, the cells were induced with 0.3 mM isopropyl-1-thio-β-D-galactopyranoside for 4 h. The virus-like particles formed (if any) were purified by using a procedure similar to that used for purification of the virus (6). Briefly, the cell pellet obtained after the induction was resuspended in 50 mM sodium citrate buffer (pH 5.5), sonicated, and the supernatant was subjected to 10% polyethylene glycol precipitation. The precipitate was resuspended in 50 mM citrate buffer (pH 5.5) and subjected to high speed pelleting. The pellet was dissolved in citrate buffer and layered onto 10–40% sucrose gradient and centrifuged at 26,000 rpm in an SW28 rotor for 3 h. The light scattering zone was collected with a Pasteur pipette, diluted, and subjected to ultra centrifugation for 3 h at 26,000 rpm. The pellet obtained was resuspended in 50 mM sodium citrate buffer (pH 5.5).

The mutant rCPs that failed to assemble were purified by Ni-NTA affinity chromatography. The cell pellet after the induction was resuspended in 100 mM Tris HCl buffer (pH 6.8) containing 300 mM NaCl and 5% glycerol. The sample was frozen at −20 °C overnight, thawed at room temperature, and sonicated for 30 min. The sample was then centrifuged at 27,000 × *g* for 15 min to remove the insoluble debris. The soluble fraction was mixed with 2 ml of Ni-NTA resin pre-equilibrated with the same buffer and allowed to rotate in an end-to-end rocker for ~2 h. The protein resin complex was washed extensively with 100 mM Tris-HCl (pH 6.8) containing 300 mM NaCl, 60 mM imidazole, and 5% glycerol. The protein was eluted with 100 mM Tris-HCl (pH 6.8) containing 300 mM NaCl, 250 mM imidazole, and 5% glycerol. The purity of the mutant rCPs thus obtained was checked by 12% SDS-PAGE (12).

Western Blot Analysis—The mutant rCPs were separated on SDS 12% acrylamide gel and transferred onto nitrocellulose membranes (13). The Western blot analysis was carried out using a monoclonal antibody (PA3B2) specific for CP as the primary antibody and goat antimouse IgG conjugated to horseradish peroxidase as the secondary antibody as described earlier (14). The blot was developed using diamino benzidine in the presence of hydrogen peroxide in 0.05 M sodium citrate buffer (pH 4.8) containing trace amounts of cobalt chloride.

Gel Filtration Analysis—The wild type and mutant rCPs were analyzed on a Bio-Sil 400 gel filtration column using the Shimdzu LC6A system. The column was equilibrated with the Tris-HCl buffer (pH 6.8) containing 300 mM NaCl and 5% glycerol. The column was calibrated with standard molecular weight markers supplied by Bio-Rad.

Circular Dichroism—CD spectra of protein samples (0.2 mg/ml) in 0.1 M Tris-HCl buffer (pH 6.8) containing 200 mM NaCl and 5% glycerol were recorded on a Jasco-715 spectropolarimeter (Japan Spectroscopic Co., Tokyo, Japan) at room temperature (25 °C).

Thermal stability of the rCP and its mutants was assessed using CD by following the changes in the secondary structure as a function of temperature. The CD measurements were carried out in a Jasco-810 spectropolarimeter (Japan Spectroscopic Co., Tokyo, Japan) using a bandwidth of 1 nm and a response time of 1 s in a cuvette with a 0.2-cm path length. The protein samples (0.2–0.3 mg/ml in 100 mM, Tris-HCl (pH 6.8) containing 200 mM NaCl and 5% glycerol) were heated from 25–95 °C at the rate of 1 °C/min. The thermal unfolding was monitored at 222 nm, and the ellipticity observed was used to calculate molar ellipticity ([θ]) as seen in Equation 1,

$$[\theta] = \theta \times 100 \times M_r/c \times l \qquad (\text{Eq. 1})$$

where θ is measured ellipticity, M_r is protein molecular weight, c is the concentration of the protein in milligrams per milliliter, and l is the path length in centimeters.

Fluorescence—Fluorescence measurements were recorded on a SPEX FluoroMax-3 Spectrofluorimeter in a 1-ml cuvette with a path length of 1 cm at 25 °C. For measuring the intrinsic fluorescence, the protein was excited at 280 nm, and the emission spectrum was recorded between 300 and 400 nm. In the case of urea-induced unfolding experiments, the fluorescence intensities were recorded at 324 nm, where the difference between partially folded (untreated) and 8 M urea treated proteins was maximum. The readings were converted to relative fluorescence and plotted against urea concentration. In all the experiments the protein concentration was 0.2 mg/ml in 0.1 M Tris-HCl buffer (pH 6.8) containing 200 mM NaCl and 5% glycerol at room temperature (25 °C).

8-Anilino-1-naphthalenesulfonate (ANS) Binding—ANS binding was monitored by measuring the fluorescence intensities between 440 and 540 nm after excitation at 370 nm. In the case of urea unfolding, the proteins (0.2 mg/ml) were incubated at various concentrations of urea for 2 h at 25 °C. ANS was added to the protein samples to a final concentration of 10 μM. The samples were excited at 370 nm, and ANS binding was monitored by measuring the fluorescence emission at 470 nm. The readings were converted to relative fluorescence and plotted against urea concentration.

Fluorescence Quenching by Acrylamide and Potassium Iodide—Fluorescence measurements of rCP and its mutants in the presence of increasing concentrations of acrylamide/iodide (0–0.5M) were recorded on a SPEX FluoroMax-3 Spectrofluorimeter in a 1-ml cuvette with a path length of 1 cm at 25 °C. The fluorescence intensity was recorded at 324 nm after excitation at 280 nm. The fractional quenching (F_0/F) was plotted against acrylamide/iodide concentration (Stern-Volmer plot), where F_0 and F represent the fluorescence in the absence and presence of acrylamide/iodide, respectively. In all experiments, the protein concentration was 0.2 mg/ml in 0.1 M Tris-HCl buffer (pH 6.8) containing 200 mM NaCl and 5% glycerol at room temperature (25 °C).

Light Scattering Measurements of Urea Unfolded rCP—Purified rCP capsids were incubated with 0–8 M urea at room temperature for 4–5 h. The absorbance was recorded at 325 nm.

RESULTS

Expression and Characterization of Site-specific Mutants of rCP—The site-specific mutants Q37E, Y67A, R68Q, D83A, I123A, and S145A were generated by the PCR-based sense and antisense primer method (11). The mutant clones were sequenced by Sanger's dideoxy chain termination method to confirm the presence of the desired mutation (15). The mutants were overexpressed in *E. coli* BL21 (DE3) pLys S (16). All of the mutants were expressed to high levels (25–30% of the total proteins) and were partially soluble. Approximately 60% of I123A and S145A were present in the soluble fraction. The solubility of the other mutant rCPs varied depending on the expression level in different batches. On average, ~10–15% of the expressed protein was present in a soluble fraction (data not shown). The mutant proteins present in the soluble fractions were purified by the procedure similar to that used for the purification of wild type rCP capsids (6). The rCP expressed in *E. coli* has 41 additional amino acid residues (including six histidines) at the N terminus and, as shown earlier (8), it assembled into capsids that sedimented as a single peak when subjected to sucrose density gradient centrifugation (fractions 12–16; Fig. 1*a*). The S145A mutant rCP co-sedimented with rCP capsids (Fig 1*b*). However, none of the other mutant proteins exhibited peaks corresponding to assembled particles (Fig. 1*a*). Furthermore, no assembled particles were seen when these mutant proteins were viewed under the electron microscope, whereas particles of 30 nm were observed for the mutant S145A capsids (Fig. 1*b*, *inset*). The mutant rCPs that failed to assemble into T = 3 capsids could not be purified by the procedures used for the purification of rCP capsids. Hence, these mutant proteins were purified by Ni-NTA chromatography, making use of the histidine tag at the N terminus. The purified proteins were analyzed by 12% SDS-polyacrylamide gel and were authenticated by Western blot analysis (data not shown). The yields of the purified proteins were 10–15 mg/liter for Q37E, Y67A, R68Q, and D83A rCPs, whereas it was slightly higher (20–25 mg/liter) for the I123A rCP. These purified proteins were also observed under an electron microscope, which further confirmed that these mutant rCPs failed to assemble
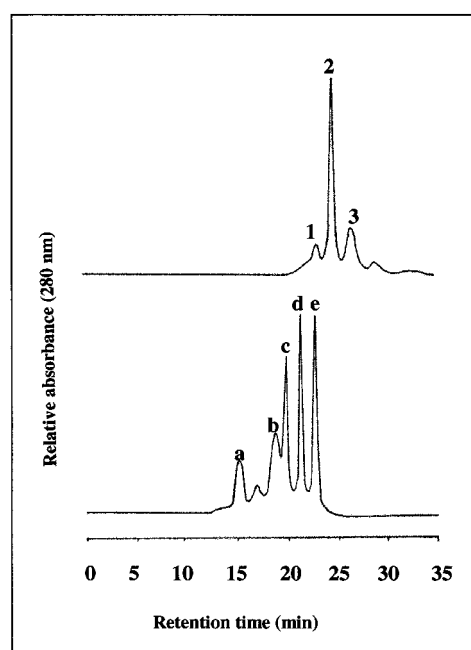
a

b
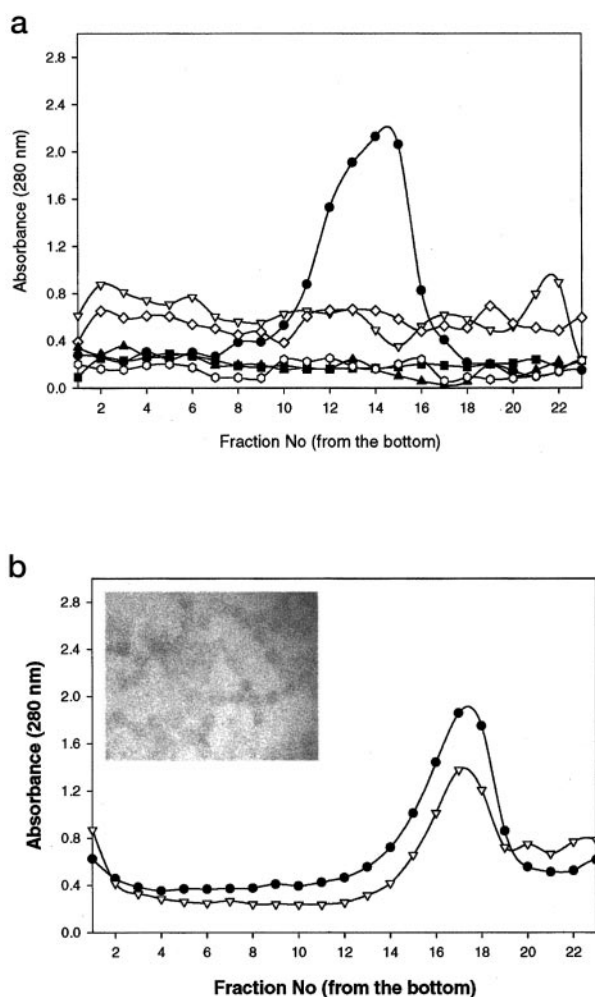
FIG. 1. **Sucrose gradient analysis of the recombinant capsids.** *a*, rCP and its mutants were layered onto a 10–40% sucrose gradient and centrifuged at 26,000 rpm for 3 h using an SW 28 rotor. 1-ml fractions were collected from the bottom of the tubes, and the absorbance at 280 nm was measured. rCP, Q37E, Y67A, R68Q, D83A and I123A rCPs are shown as ●, ▽, ■, ◇, ▲, and ○, respectively. *b*, sucrose gradient analysis of rCP and S145A capsids. rCP and S145A capsids mutants were layered onto a 10–40% sucrose gradient and centrifuged at 26,000 rpm for 2.5 h using an SW 28 rotor. 1-ml fractions were collected from the bottom of the tubes, and the absorbance at 280 nm was measured. rCP and S145A rCP are shown as ● and ▽, respectively. The *inset* shows the electron micrograph of S145A capsids.

FIG. 2. **Size-exclusion chromatography of the rCP mutant.** The I123A mutant (*upper panel*) was run on a Bio-SIL 400 column calibrated previously with molecular mass markers (*bottom panel*). Peaks *a*, *b*, *c*, *d*, and *e* correspond to thyroblobulin (670 kDa), IgG (150 kDa), ovalbumin (44 kDa), myoglobin (17 kDa), and vitamin B_{12} (1.3 kDa) respectively. The *top panel* shows the elution profile of I123A. The peaks *1*, *2*, and *3* obtained were authenticated by Western analysis. Similar gel filtration profiles were obtained for the Y67A, R68Q, D83A, and I123A mutants (data not shown).

FIG. 3. **Far UV CD spectra of purified rCP and its mutants.** CD measurements were made using Jasco Spectropolarimeter. The spectra were recorded between 200 and 280 nm at room temperature (25 °C). rCP, Q37E, Y67A, R68Q, D83A, and I123A mutant rCPs are shown as *solid* (—), *long dashed* (— —), *medium dashed* (– – –), *short dashed* (- - -), *dotted* (⋯), and *dash-dot-dash* (—·—) *lines*, respectively.
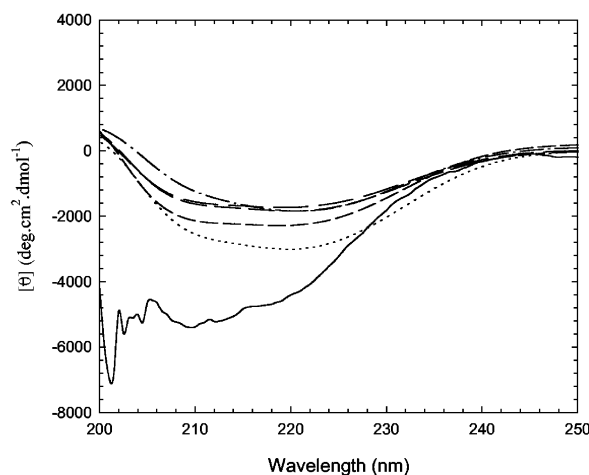
into virus-like particles. These purified mutants rCPs were retained in the loading wells when run on 1% agarose gel and 8% native polyacrylamide gels (data not shown), suggesting that these may represent proteins that are folding defective.

Oligomeric Status of rCP Mutant Proteins—Purified rCP capsids and the mutant rCPs were loaded onto a Bio-Sil 400 gel filtration column. The column was calibrated with standard protein molecular weight markers. The rCP capsids eluted immediately after the void volume as expected. However, the I123A mutant rCP behaved abnormally and eluted after vitamin B12 (Fig. 2). All of the three peaks in Fig. 2 were confirmed to be I123A mutant rCP by Western blot analysis (data not shown). The Q37E, Y67A, R68Q, and D83A mutant rCPs also behaved in a similar manner. S145A rCP capsids co-eluted with rCP capsids (data not shown). Therefore, it is likely that Q37E, Y67A, R68Q, D83A, and I123A rCP mutants exist as partially folded monomers that bind to the column and are eluted later in the run.

rCP Mutants (Q37E, Y67A, R68Q, D83A, and I123A) Exist in a Partially Folded State—Far UV CD was used to examine the

secondary structural features of the mutant rCPs that failed to assemble into capsids. The far UV CD spectra of these mutants showed troughs in the 208–225 nm range, suggesting that all of them had a considerable amount of secondary structure (Fig. 3). Furthermore, the fluorescence emission spectra of these mutants showed an emission maxima at 332–336 nm and was similar to that observed with the rCP capsids (Fig. 4*a*). This indicated that the aromatic residues, especially the single tryptophan residue, was inaccessible to the solvent. Upon incubation with 8 M urea, the emission maximum shifted to 350–356 nm, suggesting that the tryptophan side chain was exposed to

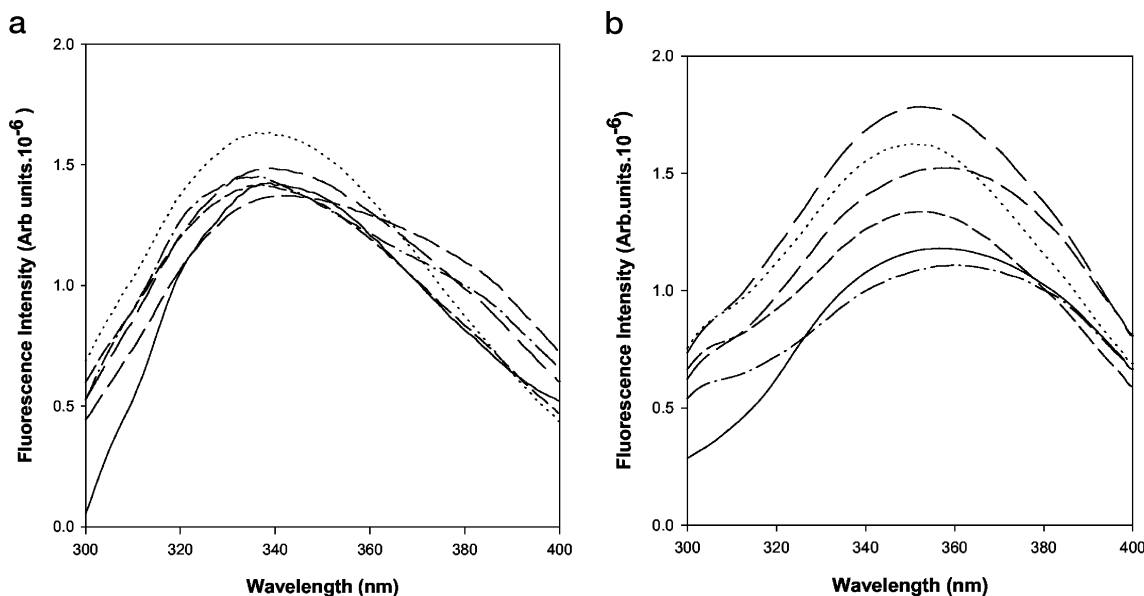*Effects of Interfacial Residue Mutations on PhMV*

FIG. 4. **Fluorescence emission spectra of rCP capsids and its mutants.** *a*, 0.2 mg/ml protein was excited at 280 nm, and emission was monitored between 300 and 400 nm. rCP, Q37E, Y67A, R68Q, D83A, and I123A are shown as *solid* (—), *long dashed* (— —), *medium dashed* (– – –), *short dashed* (- - -), *dotted* (⋯), and *dash-dot-dash* (—·—) *lines*, respectively. *b*, fluorescence emission spectra of rCP capsids and its mutants in the presence of 8 M urea. 0.2 mg/ml protein was incubated in a buffer containing 8 M urea for 2 h at room temperature, excited at 280 nm, and emissions were monitored between 300 and 400 nm. rCP, Q37E, Y67A, R68Q, D83A and I123A rCP mutants are shown as *solid* (—), *long dashed* (— —), *medium dashed* (– – –), *short dashed* (- - -), *dotted* (⋯), and *dash-dot-dash* (—·—) *lines*, respectively.
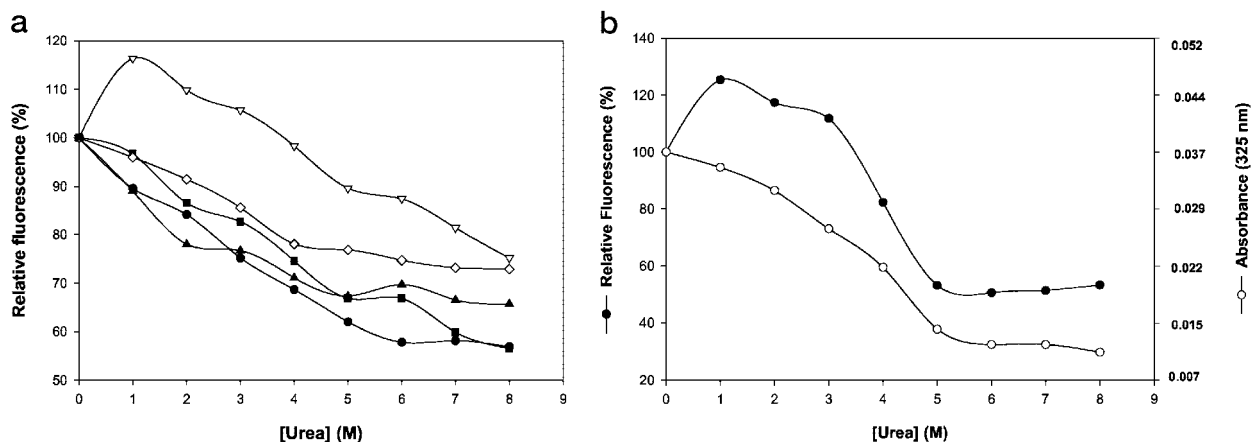

FIG. 5. **Urea denaturation studies of rCP and its mutants.** *a*, purified rCP mutants were treated with 0–8 M urea for 2 h at 25 °C. Protein was excited at 280 nm, and the emission was monitored at 324 nm. Fluorescence at 0 M urea was taken as 100%, and the relative fluorescence calculated was expressed as a function of urea concentration. Q37E, Y67A, R68Q, D83A, and I123A mutant rCPs are shown as ●, ▽, ■, ◇, and ▲, respectively. *b*, urea denaturation of rCP capsids. Purified rCP capsids were treated with 0–8 M urea, and the fluorescence was monitored as described above in *panel a*. Fluorescence emission of the tryptophan at 324 nm (*closed circles* and *left axis*) and light scattering measurements at 325 nm (*open circles* and *right axis*) are indicated.

the solvent (Fig. 4*b*). The fluorescence intensity was measured at 324 nm, at which the maximum difference in intensity was observed between the native (0 M urea) and 8 M urea unfolded proteins. The fluorescence intensities at various concentrations of urea were calculated as a percent of the fluorescence intensity at 0 M urea. A discrete unfolding transition was found between 3 to 5 M urea in the case of rCP capsids (Fig. 5*b*), whereas no such transition was observed with the mutants rCPs (Fig. 5*a*). This observation corroborates earlier studies in which the rCP capsids were found to be stable up to 4 M urea at room temperature (7). Interestingly, the urea-induced denaturation of the rCP capsids, as measured by fluorescence, overlapped with the changes in light scattering as monitored by absorbance at 325 nm (Fig. 5*b*). This indicated that disassembly and denaturation could be concerted events in this virus. The lack of a discrete unfolding transition in the case of rCP mutants as monitored by fluorescence reflects conformational

flexibility of these mutant proteins. Furthermore, the absorbance at 325 nm for the mutant rCPs (0.2 mg/ml) was negligible (<0.005), suggesting that the spectral changes observed are not due to aggregation.

The accessibility of tryptophan residues in the mutant rCPs was further assessed by quenching experiments with acrylamide and potassium iodide. Stern-Volmer plots for the wild type and mutant rCPs (Fig. 6*a*) showed a similar slope for Y67A, R68Q, and I123A mutant proteins, suggesting that the tryptophan in these proteins are protected from the quencher to a similar extent. The tryptophan in Q37E and D83A mutant rCPs, however, seemed to be more accessible. Similarly, when potassium iodide was used as a quencher, subtle differences in the accessibility of tryptophan in the mutants could be observed. Although rCP, I123A, and D83A had similar slopes, Q37E, Y67A, and R68Q showed increased slopes (Fig. 6*b*).
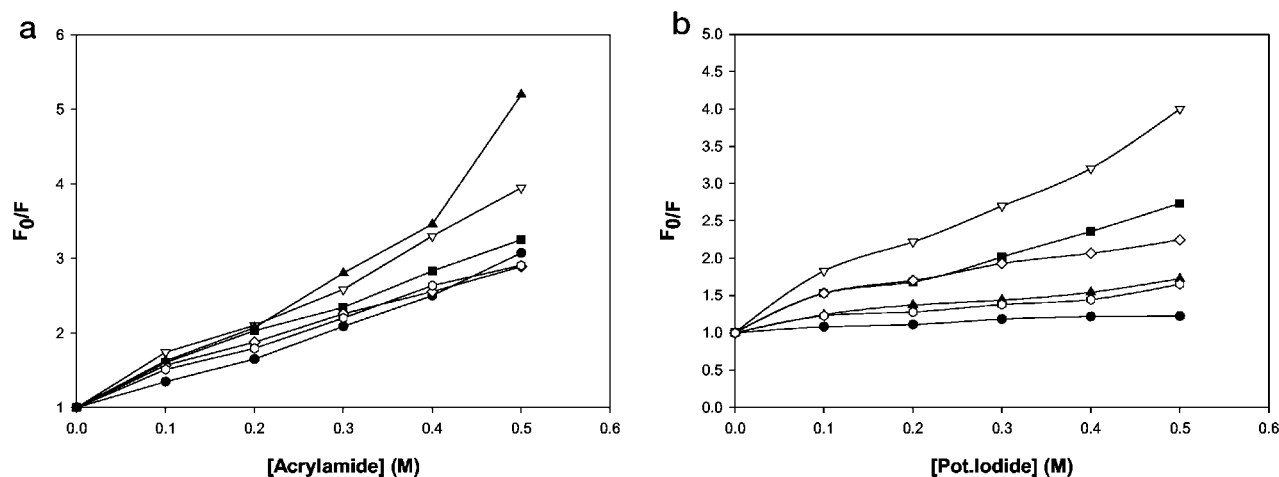
FIG. 6. **Stern-Volmer plot of tryptophan fluorescence quenching by acrylamide.** *a*, purified rCP capsids and rCP mutants were treated with 0–0.5 M acrylamide. The proteins were excited at 280 nm, and the emission was recorded at 324 nm. Fractional quenching F_0/F is plotted as a function of acrylamide concentration, where F_0 and F represent the fluorescence in the absence and presence of acrylamide, respectively. rCP capsids, Q37E, Y67A, R68Q, D83A, and I123A mutant rCPs are shown as ●, ▽, ■, ◇, ▲, and ○, respectively. *b*, Stern-Volmer plot of tryptophan fluorescence quenching by iodide. Purified rCP capsids and rCP mutants were treated with 0–0.5 M iodide. The proteins were excited at 280 nm, and emission was recorded at 324 nm. Fractional quenching F_0/F is plotted as a function of acrylamide concentration, where F_0 and F represent the fluorescence in the absence and presence of iodide, respectively. rCP capsids, Q37E, Y67A, R68Q, D83A, and I123A mutant rCPs are shown as ●, ▽, ■, ◇, ▲, and ○, respectively.
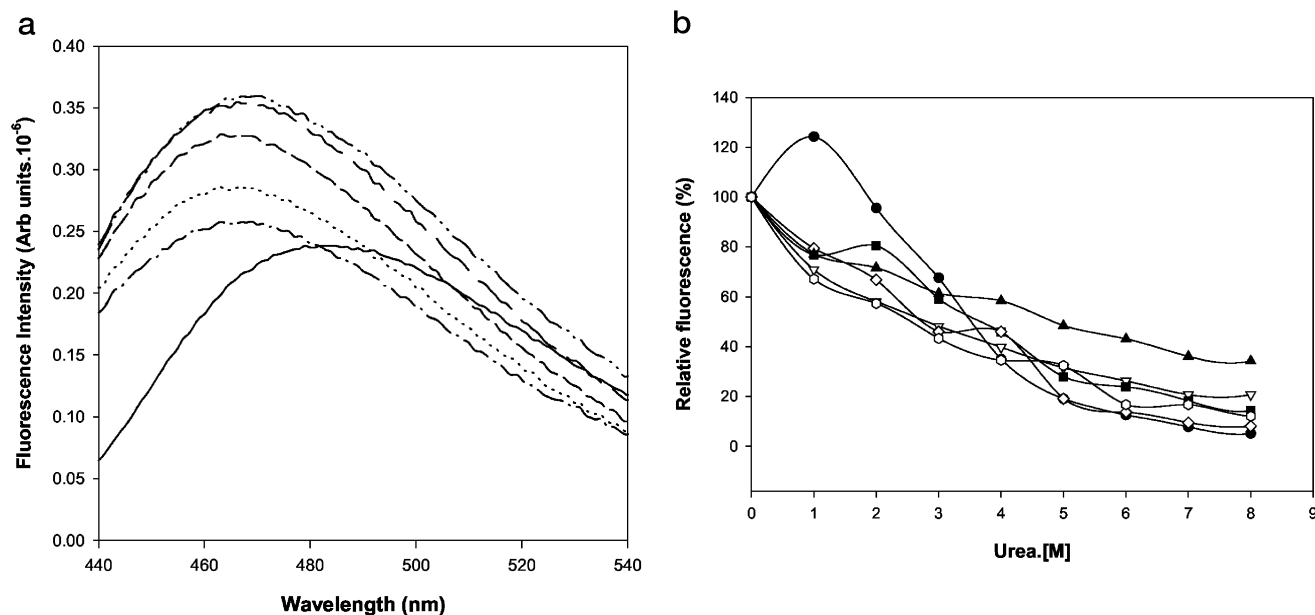

FIG. 7. **Fluorescence emission spectra of rCP capsids and rCP mutants in the presence of ANS.** *a*, ANS was added to the purified mutants (0.2 mg/ml) from a stock solution of 1 mM to a final concentration of 10 μM. The excitation wavelength was 370 nm, and fluorescence emissions were measured between 440 and 540 nm. rCP, Q37E, Y67A, R68Q, D83A, and I123A mutant rCPs are shown as *solid* (—), *dotted* (⋯), *short dashed* (- - -), *dash-dot-dot* (—··), *medium dashed* (– – –), and *dash-dot-dash* (—·—) *lines*, respectively. *b*, ANS binding to rCP capsids and rCP mutants in the presence of urea. The mutant proteins were incubated in 0–8 M urea at 25 °C for 2–3h. ANS was added to a final concentration of 10 μM. The samples were excited at 370 nm, and the fluorescence emission was monitored at 470 nm. The readings were converted to relative fluorescence and plotted against urea concentration. rCP, Q37E, Y67A, R68Q, D83A, and I123A mutant rCPs are shown as ●, ▽, ■, ◇, ▲, and ○, respectively.

Furthermore, the rCP mutants strongly bound ANS, suggesting the presence of exposed hydrophobic pockets (Fig. 7*a*). ANS binding to rCP capsids was less when compared with ANS binding to the rCP mutants (Fig. 7*a*). This is understandable, as the capsids are held by strong hydrophobic interactions and, hence, hydrophobic surfaces are unavailable for ANS to bind. The urea-induced unfolding of the rCP capsids and mutant rCPs was also monitored by measuring ANS fluorescence. As in other globular proteins, there was an initial increase (up to 3 M urea), followed by a decrease in ANS binding (up to 5 M urea) in the case of wild type rCP capsids (Fig. 7*b*). The unfolding

transition observed here is in agreement with the results of urea-induced denaturation as monitored by intrinsic fluorescence (Fig. 5*a*). In contrast, the mutant rCPs showed only a continuous decrease in ANS fluorescence, suggesting that they were already in a partially unfolded state (Fig. 7*b*).

Thermal Stability of Mutant rCPs—The partially folded nature of the mutant rCPs was further assessed by monitoring the effect of temperature on the molar ellipticity at 222 nm of the wild type and the mutant rCPs. The wild type rCP and S145A capsids exhibited a T_m of 88 and 83 °C, respectively (Fig. 8*a*). Q37E, Y67A, and R68Q mutant rCPs did not show a
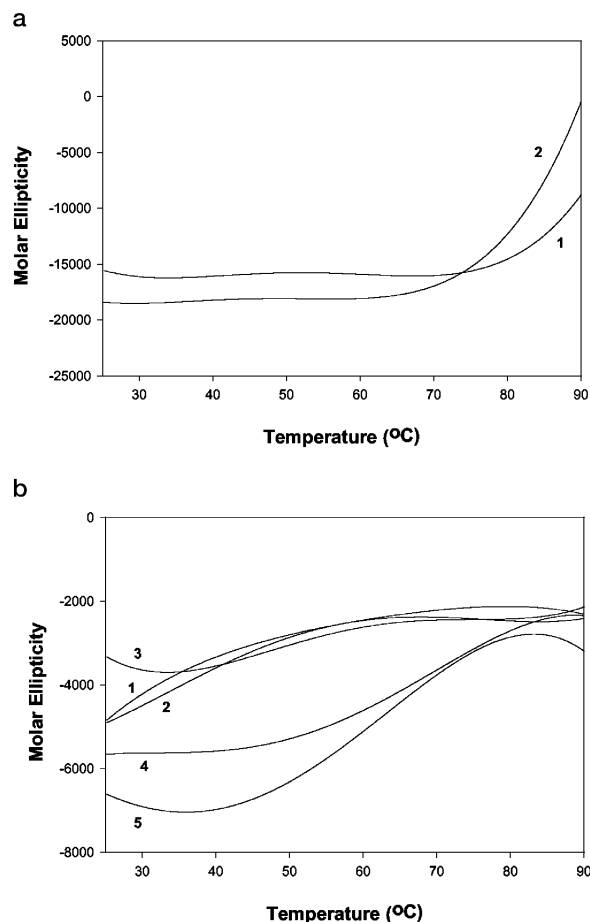
FIG. 8. **Thermal denaturation of rCP capsids and its mutants.** *a*, T_m of wild type rCP (*line 1*) and S145A rCP mutant (*line 2*) are shown. Wild type rCP has a T_m of 88 °C, whereas that of the S145A mutant rCP was found to be 83 °C. *b*, thermal denaturation of rCP mutants. The thermal scans of the Q37E (*line 1*), Y67A (*line 2*), R68Q (*line 3*), D83A (*line 4*), and I123A (*line 5*) rCP mutants are indicated.

discrete transition, whereas the D83A and I123A mutant rCPs showed a broad transition between 50 and 70 °C (Fig. 8*b*). These results further emphasize the conformational flexibility in these mutant rCPs.

DISCUSSION

We have resorted to the molecular biology approach to decipher the roles of specific amino acids in the formation of capsids of PhMV. Earlier studies by site-directed mutagenesis have shown the presence of a 19.4 S intermediate in the assembly/disassembly pathway (8). In this study, we have carried out a structure-based mutagenesis of six residues, namely Gln-37, Tyr-67, Arg-68, Asp-83, Ile-123, and Ser-145, which are predominantly involved in inter-subunit interactions. Except for S145A, all of the other mutant rCPs failed to assemble into T = 3 capsids, although they were found to be soluble (Fig. 1). Furthermore, these mutant proteins are partially folded, as evidenced by the following: (i) gel filtration elution behavior (Fig. 2); (ii) the presence of secondary structure as shown by far UV CD (Fig. 3); (iii) the lack of a sharp transition in thermal denaturation as shown by CD (Fig. 8); (iv) persistent high levels of innate fluorescence due to the single tryptophan present in the protein (Fig. 4); (v) lack of discrete unfolding transition upon denaturation with urea (Fig. 5); (vi) accessibility of tryptophan residue in the mutants as measured by fluorescence quenching with acrylamide and potassium iodide (Fig. 6); (vii) enhanced fluorescence of ANS in the presence of mutant proteins (Fig. 7); and (viii) the lack of a sharp structural transition in ANS binding experiments in the presence of urea (Fig. 7). Thus, the mutation of residues involved in extensive inter-subunit interactions affect both the subunit folding and particle assembly of PhMV. A detailed analysis of the position of the residues mutated and the probable consequence of the mutation on the folding and assembly is presented below.

Gln-37 is conserved in all of the tymoviruses and is present at hydrogen-bonding distance to the conserved glycines 113 and 114 and leucine 109, respectively, at the A-A5 interface (Fig. 9 and Fig. 10*a*). Gln-37 also interacts with Gly-113 and
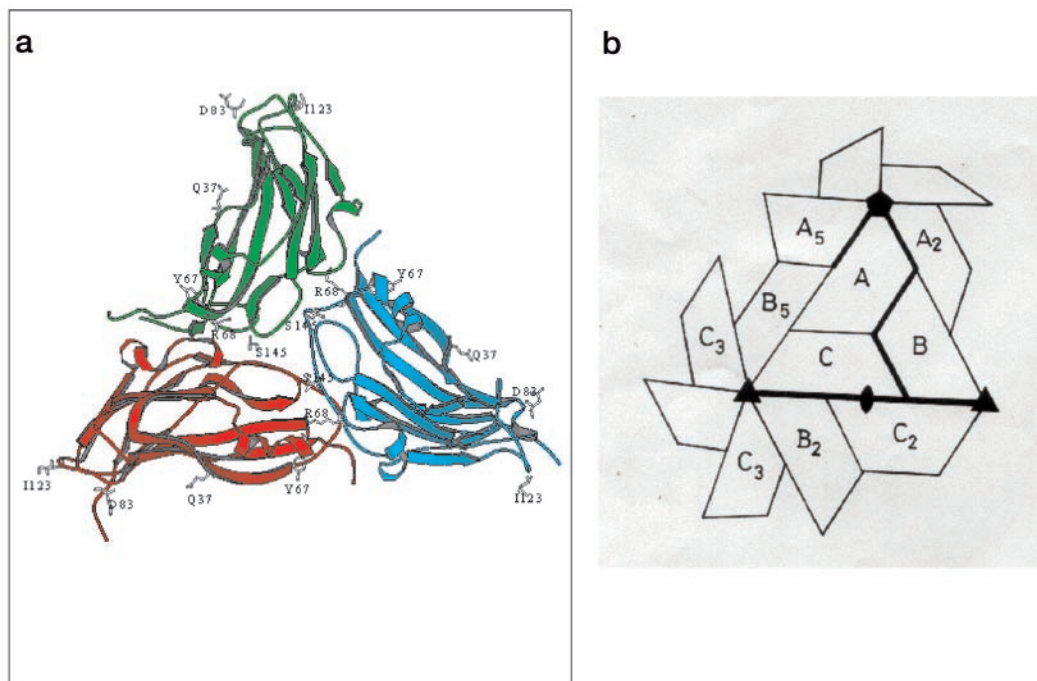
FIG. 9. **Coat protein subunits of PhMV.** *a*, ribbon diagram of the A, B, and C subunits of the PhMV coat protein in the assymetric unit showing the mutations. The A, B, and C subunits are colored *green*, *red*, and *cyan* respectively. The residues selected for mutation are indicated. *b*, diagram illustrating the convention used to designate subunits on the T = 3 capsid of PhMV. The A subunits form pentamers at the 5-fold axis, whereas the B and C subunits form hexamers at the 3-fold icosahedral axes.
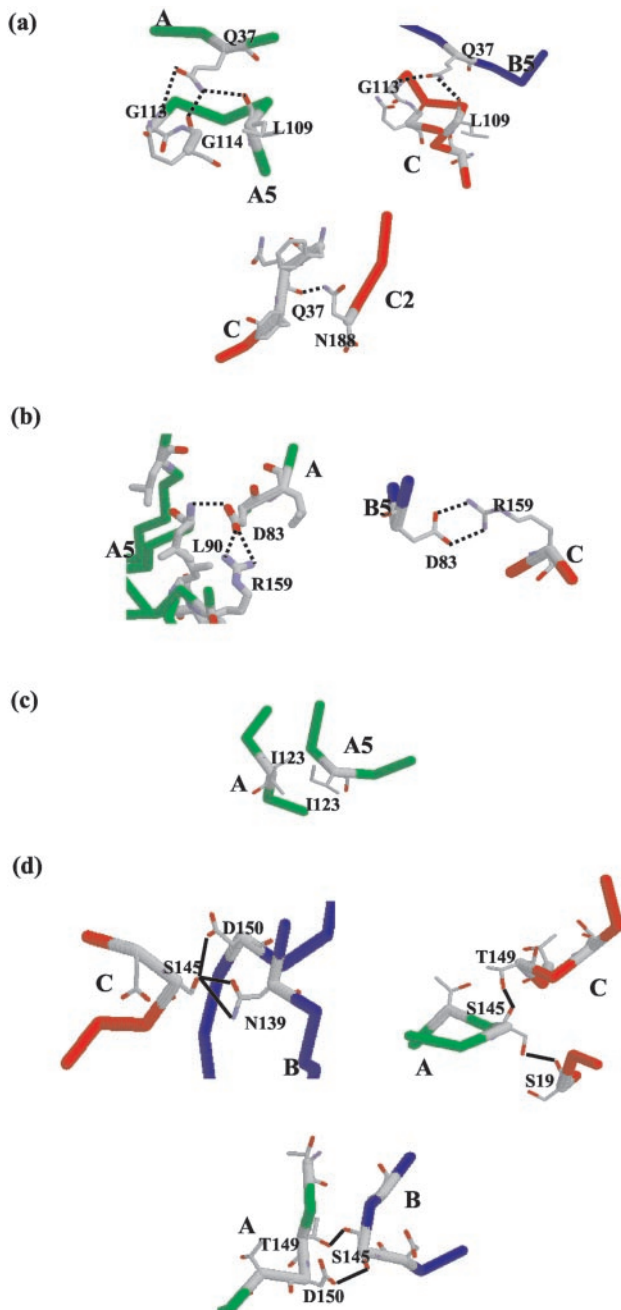
FIG. 10. **Interfacial interactions of PhMV.** *a*, interactions of Gln-37 (*Q37*) with residues from the neighboring subunits. Hydrogen bonding interactions of Gln-37 with other residues at the A-A5, B5-C, and C-C2 contacts. The A, B, and C subunits are colored in *green*, *blue*, and *red*, respectively. *b*, interaction of Asp-83 (*D83I*) with Arg-159 (*R159*) from the neighboring subunits. Asp-83 (*D83*) is involved in salt linkage with Arg (*R159*) at the A-A5 and B5-C contacts. The A, B, and C subunits are colored in *green*, *blue*, and *red*, respectively. *c*, hydrophobic interaction of Ile-123 (*I123*) with itself from the neighboring subunit at the A-A5 contact. A subunits are shown in *green*. *d*, interaction of Ser-145 (*S145*) with residues from the neighboring subunits. Interactions of Ser-145 with other residues at A-B, B-C, and C-A contacts are shown. The A, B, and C subunits are colored in *green*, *blue*, and *red*, respectively.

Leu-109 at B5-C interface and with Asn-188 at C-C2 contacts (Fig. 9 and Fig. 10a). This residue does not seem to interact with any of the residues within the subunit. The mutation of Gln-37 to Glu should therefore have disrupted only the inter-subunit interactions. Replacement of Gln with Glu in the structure using the molecular modeling software program "O" showed that there are no short contacts and also that all the

interactions of Gln-37 can be retained by Glu. However, it introduces a negative charge in the dense interface of subunits. The results presented here demonstrate that the mutation of Gln-37, which is involved in multiple inter-subunit interactions, also affects the proper folding of the subunit. Probably, the negative charge introduced somehow interferes in the folding.

Arg-68, another conserved residue in all tymoviruses, is at hydrogen-bonding distance with Asp-136, Ser-137, and Val-138 at the A-B interface and is involved in a salt bridge with Asp-150 at the B-C interface (Fig. 9). This residue does not have any obvious intra-subunit interactions. The replacement of Arg with Gln can be done without short contact within the same subunit. However, its mutation to Gln led to the partially folded and assembly-incompetent protein. These results further support the observation that the mutation of residues involved in multiple inter-subunit interactions disrupts subunit folding and particle assembly. Even here, the uncompensated negative charge might interfere in the folding of the protein.

Asp-83 and Ile-123, although not conserved among all tymoviruses, are involved in extensive interactions with residues from the other subunits (Fig. 10, *b* and *c*). The mutation of these two residues to alanine also led to the partially folded proteins that were assembly-incompetent.

Tyr-67 is also conserved across the tymovirus group. It is involved not only in inter-subunit interactions at C-C2 and B5-A, but also in intra-subunit hydrogen-bonding interactions. Its mutation to alanine disrupts the hydrogen-bonding interaction at the quasi-2-fold axis. This creates a cavity in the vicinity of residues Leu-34, Leu-63, Leu-180, and Ile-32. This may have a destabilizing effect on the same subunit, which could hinder proper folding of the subunit. Hence, its mutation to Ala led to the misfolding of the subunits and the consequent arrest of assembly.

Interestingly, the tertiary structure of the partially folded mutant proteins is similar to that of the rCP capsids (Figs. 4 and 6). The single tryptophan residue, Trp-96, is located inside the β-barrel, and its mutation led to soluble aggregates defective in folding and assembly (8). Furthermore, this Trp is not an interfacial residue. Therefore, it is possible that the partially folded mutant rCPs and the wild type rCP have similar accessibility to this tryptophan.

In contrast to the Q37E, Y67A, R68Q, D83A, and I123A mutant rCPs, the S145A mutant assembled into capsids that were indistinguishable from wild type rCP capsids. An analysis of the intact PhMV capsid structure shows that Ser-145 has hydrogen-bonding interactions with Thr-149 and Asp-150 in the A-B interface, Ser-19 and Thr-149 at the A-C interface, and Asp-150 and Asn-139 at the B-C interface (Fig. 10d). These interactions are presumably less important or are compensated by other interactions in the mutant rCP and thus do not affect the folding or assembly. Earlier studies on D144N, N188Δ1, and N188A mutant rCPs have shown that they do assemble into capsids, although these residues occur at the inter-subunit interfaces (8). Thus, none of the mutant proteins studied thus far has resulted in a fully folded and assembly-competent monomeric subunit. It is, however, possible that the mutant rCPs are not correctly folded when synthesized *in vivo* and hence are assembly incompetent. To examine this, the wild type rCP capsids were incubated with 8 M urea for 4 h at room temperature and subjected to stepwise dialysis or immediate dilution (20-fold) to remove the denaturant. However, it was not possible to obtain assembled particles from such refolding mixtures. Invariably, the removal of denaturant led to the complete precipitation of the

protein. Because it was not possible to refold and assemble the wild type rCP, similar experiments with mutant rCPs were not attempted. *In vivo* studies on the related turnip yellow mosaic virus has shown that the coat protein synthesized in the endoplasmic reticulum accumulates in the cytoplasm overlying clustered vesicles in the chloroplast (17). These become inserted into the outer chloroplast membrane with the hydrophobic sides that are normally buried in the complete virus particle within the lipid bilayer. It is suggested that the nascent RNA strand emerges through the vesicle neck and that virus assembly takes place in the vesicular membrane (17). Thus, the partially folded CP attached to the membrane, upon interaction with RNA, could further fold and assemble into mature capsids. In the absence of RNA, these proteins might self-assemble to form empty capsids. The results presented in this communication clearly demonstrate that the mutation of residues crucial for interfacial interactions disrupts subunit folding and assembly in the PhMV. Furthermore, these mutants are partially folded and are probably locked in conformations that lack the signals/features that would allow them to assemble into T = 3 capsids. The unfolding transition, as monitored by fluorescence, overlapped with the changes in the light scattering when wild type rCP capsids were denatured with urea, suggesting that disassembly and unfolding are also concerted (Fig. 5*b*). Thus, there is a close connection between folding and assembly in PhMV. In the flock house virus also, the disassembly and unfolding of the mature capsids was shown to be concerted (18). Viral structural proteins, such as the herpes simplex virus triplex forming protein (VP23), when expressed in *E. coli*, are shown to exist predominantly in a molten globule state (19). The P22 coat protein has also been shown to be quite flexible in solution (20). Thus, concerted coat protein folding and capsid assembly may be a general phenomenon in viruses stabilized predominantly by inter-subunit interactions.

REFERENCES

1. Ranjith-Kumar, C. T., Gopinath, K., Jacob, A. N. K., Srividhya, V., Elango, P., and Savithri, H. S. (1998) *Arch. Virol.* **143,** 1489–1500
2. Harrison, S. C., Olson, A. J., Schutt, C. E., Winkler, F. K., and Bricogne, G. (1978) *Nature* **276,** 368–373
3. Kaper, J. M. (1975) *The Chemical Basis of Virus Structure, Dissociation, and Assembly*, Vol. 39, North-Holland Publishing Co., Amsterdam
4. Katouzian-Safadi, M., Favre, A., and Haenni, A. L. (1980) *Eur. J. Biochem.* **112,** 479–486
5. Katouzian-Safadi, M., and Berthet-Colominas, C. (1983) *Eur. J. Biochem.* **137,** 47–53
6. Savithri, H. S., Munshi, S. K., Suryanarayana, S., Divakar, S., and Murthy, M. R. N. (1987) *J. Gen. Virol.* **68,** 1533–1542
7. Sastri, M., Kekuda, R., Gopinath, K., Ranjith Kumar, C. T., Jagath, J. R., and Savithri, H. S. (1997) *J. Mol. Biol.* **272,** 541–552
8. Sastri, M., Reddy, D. S., Krishna, S. S., Murthy, M. R. N., and Savithri, H. S. (1999) *J. Mol. Biol.* **289,** 905–918
9. Krishna, S. S., Hiremath, C. N., Munshi, S. K., Prahadeeswaran, D., Sastri, M., Savithri, H. S., and Murthy, M. R. (1999) *J. Mol. Biol.* **289,** 919–934
10. Krishna, S. S., Sastri, M., Savithri, H. S., and Murthy, M. R. N. (2001) *J. Mol. Biol.* **307,** 1035–1047
11. Weiner, M. P., Costa, G. L., Schoettlin, W., Cline, J., Mathur, E., and Bauer, J. C. (1994) *Gene* **151,** 119–123
12. Laemmli, U. K. (1970) *Nature* **227,** 680–685
13. Towbin, H., Staehelin, T., and Gordon, J. (1979) *Proc. Natl. Acad. Sci. U. S. A.* **76,** 4350–4354
14. Kekuda, R., Karande, A. A., Jacob, A. N. K., and Savithri, H. S. (1993) *Virology* **193,** 959–966
15. Sanger, F., Nicklen, S., and Coulson, A. R. (1977) *Proc. Natl. Acad. Sci. U. S. A.* **74,** 5463–5467
16. Studier, F. W., and Moffatt, B. A. (1986) *J. Mol. Biol.* **189,** 113–130
17. Matthews, R. E. F. (1991) *Plant Virology,* 3rd Ed., pp. 231–239, Academic Press, New York
18. Oliveira, A. C., Gomes, A. M. O., Almeida, F. C. L., Mohana-Borges, R., Valente, A. P., Reddy, V. S., Johnson, J. E., and Silva, J. L. (2000) *J. Biol. Chem.* **275,** 16037–16043
19. Kirkitadze, M. D., Barlow, P. N., Price, N. C., Kelly, S. M., Boutell, C. J., Rixon, F. J., and McClelland, D. A. (1998) *J. Virol.* **72,** 10066–10072